Toxicology Letters 338 (2021) 10–20

Contents lists available at ScienceDirect

Toxicology Letters

journal homepage: www.elsevier.com/locate/toxlet

Meloxicam methyl group determines enzyme specificity for thiazole bioactivation compared to sudoxicam

Dustyn A. Barnette[a], Mary A. Schleiff[a], Arghya Datta[b], Noah Flynn[b], S. Joshua Swamidass[b], Grover P. Miller[a,*]

[a] Department of Biochemistry and Molecular Biology, University of Arkansas for Medical Sciences, 4301 W Markham St, Little Rock, AR, 72205, United States
[b] Department of Pathology and Immunology, 660 S Euclid Ave, Washington University, St. Louis, MO, 63130, United States

HIGHLIGHTS

- Quantitative kinetics revealed enzyme roles in meloxicam/sudoxicam metabolism.
- Thiazole methyl substituent alters enzyme specificity for bioactivation.
- CYP1A2 dominates meloxicam bioactivation and CYP2C9 its detoxification.
- CYP2C8 dominates sudoxicam bioactivation.
- P450 s dominating competing meloxicam pathways implicate possible roles in toxicity.

GRAPHICAL ABSTRACT

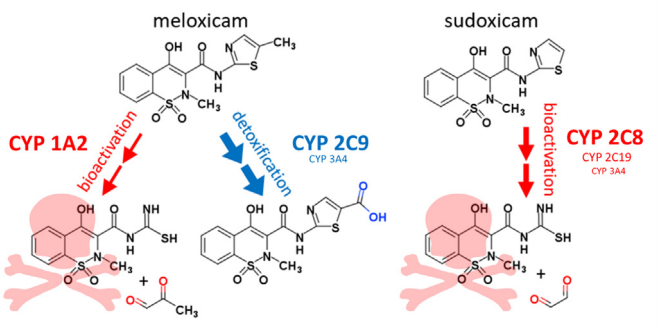

ARTICLE INFO

Article history:
Received 18 August 2020
Received in revised form 12 November 2020
Accepted 17 November 2020
Available online 27 November 2020

Keywords:
Sudoxicam
Meloxicam
NSAID
Cytochrome P450
Thiazole
Epoxidation
Bioactivation
Toxicity
Liver
DILI

ABSTRACT

Meloxicam is a thiazole-containing NSAID that was approved for marketing with favorable clinical outcomes despite being structurally similar to the hepatotoxic sudoxicam. Introduction of a single methyl group on the thiazole results in an overall lower toxic risk, yet the group's impact on P450 isozyme bioactivation is unclear. Through analytical methods, we used inhibitor phenotyping and recombinant P450s to identify contributing P450s, and then measured steady-state kinetics for bioactivation of sudoxicam and meloxicam by the recombinant P450s to determine relative efficiencies. Experiments showed that CYP2C8, 2C19, and 3A4 catalyze sudoxicam bioactivation, and CYP1A2 catalyzes meloxicam bioactivation, indicating that the methyl group not only impacts enzyme affinity for the drugs, but also alters which isozymes catalyze the metabolic pathways. Scaling of relative P450 efficiencies based on average liver concentration revealed that CYP2C8 dominates the sudoxicam bioactivation pathway and CYP2C9 dominates meloxicam detoxification. Dominant P450s were applied for an informatics assessment of electronic health records to identify potential correlations between meloxicam drug-drug interactions and drug-induced liver injury. Overall, our findings provide a cautionary tale on assumed impacts of even simple structural modifications on drug bioactivation while also revealing specific targets for clinical investigations of predictive factors that determine meloxicam-induced idiosyncratic liver injury.

* Corresponding author.
E-mail address: MillerGroverP@uams.edu (G.P. Miller).

http://dx.doi.org/10.1016/j.toxlet.2020.11.015
0378-4274/

1. Introduction

The incorporation of substituents on a thiazole ring renders the substructure selective for a wide variety of biological targets (Kumar et al., 2016) and thus, leads to applications for many drug classes including anticancer, antimicrobial, anticonvulsant, and anti-inflammatory agents (Ayati et al., 2015). Nevertheless, these modifications may introduce the capacity of some thiazole-containing drugs to elicit idiosyncratic drug-induced liver toxicity (Jean and Fotsch, 2012). The proposed bioactivation pathway involves epoxidation of the thiazole C4-C5 double bond (Scheme 1). Hydrolysis of the epoxide yields an unstable diol that cleaves the ring to form a thioamide and α-dicarbonyl cometabolite (Mizutani et al., 1994; Dalvie et al., 2002). The thioamide is a protoxin, whose subsequent metabolism causes the toxic response (Mizutani et al., 1992; Neal and Halpert, 1982; Kedderis, 2020). Despite elucidation of this pathway, the impact of structural modifications on thiazole bioactivation are not well understood. The realistic but unpredictable risk of bioactivation justifies thiazole labeling as a "structural alert" that requires further study to resolve this uncertainty.

The story of the nonsteroidal anti-inflammatory drugs (NSAID) sudoxicam and Mobic (meloxicam) epitomizes the challenges in predicting bioactivation and hence toxic risk for thiazole-containing drugs. Only a methyl group at the C5 position of the thiazole ring differentiates meloxicam from sudoxicam, but the substitution makes a critical difference on the path to the clinic. In the early 1970s (Wiseman and Chiaini, 1972), sudoxicam was reported as a member of a promising new class of NSAIDs. Nevertheless, subsequent clinical trials were discontinued due to multiple deaths related to hepatotoxicity (Roth, 2001), so that sudoxicam was never approved for marketing. Eventually, studies implicated thiazole bioactivation as the source of reactive metabolites capable of initiating toxic responses arising from sudoxicam exposure (Obach et al., 2008; Zhang, 2014). Nearly 30 years later, introduction of a methyl group transformed sudoxicam to meloxicam, which proved to be a much safer NSAID. Unlike sudoxicam, meloxicam use causes rare, but significantly elevated aminotransferase levels (> 3-fold) in patients (0.2–1 %) ("LiverTox," 2018; Rostom et al., 2005), and for individual cases, there are incidences of clinically apparent livery injury ("LiverTox," 2018; Staerkel and Horsmans, 1999). Given those minor risks, meloxicam was approved to treat osteoarthritis in 2000 (Yocum et al., 2000) and later for more severe rheumatoid arthritis in 2004 (Ahmed et al., 2005; Gabriel et al., 1996). These advances in the drug market resulted in access to the first NSAID preferentially targeting COX-2 and thus causing fewer gastrointestinal adverse effects compared to other NSAIDs (Ahmed et al., 2005).

The better safety profile for meloxicam over sudoxicam is attributable to the methyl group as the only difference between the drugs; however, a mechanistic explanation is not that obvious. Empirical evidence suggests that the C5 position is a structural "soft spot" for thiazole bioactivation, so that the incorporation of functional groups prevents drug induced toxicity (Jean and Fotsch, 2012). In the case of meloxicam, the methyl group creates a detoxification pathway inaccessible to sudoxicam and thus, suppresses meloxicam bioactivation (Obach et al., 2008; Barnette et al., 2020). Moreover, the methyl group surprisingly decreases the efficiency of the bioactivation pathway (Barnette et al., 2020). The combined effect is a 15-fold lower bioactivation of meloxicam relative to sudoxicam based on studies with pooled human liver microsomes as a model for the average adult. The actual relevance of meloxicam and sudoxicam bioactivations will ultimately depend on currently unknown specific enzymes catalyzing reactions and their variation in the general population.

Herein, we identified cytochrome P450 isozymes responsible for catalyzing meloxicam and sudoxicam bioactivation and detoxification and assessed their potential importance in determining toxicity outcomes. Initially, we identified P450s contributing to metabolism using inhibitor phenotyping of human liver microsomes and specific activity reactions with recombinant P450 s. These enzymes were targeted for steady-state studies to determine mechanisms and constants for bioactivation and detoxification pathways. We then used the *in vitro* kinetic data to extrapolate P450 *in vivo* clearance and contributions for an average adult as a model for their potential clinical relevance. Clinical factors impacting relative roles of P450s involved in meloxicam bioactivation and detoxification could lead to patterns in patient data associated with liver injury. Consequently, we conducted an exploratory investigation for evidence of drug-drug interactions with meloxicam and liver injury present in electronic health records from the BJC HealthCare network at St. Louis using deep neural networks.

2. Materials and methods

2.1. Materials

Chemical solvents (methanol, acetonitrile, and DMSO) and $MgCl_2$ were obtained from Thermo Fisher Scientific (Waltham, MA). Millipore-Sigma (Burlington, MA) was the source for the following: meloxicam (substrate), glyoxal and methylglyoxal (metabolite standards), 7-hydroxycoumarin (internal standard), cytochrome P450 isozyme inhibitors (1-aminobenzotriazole, α-naphthoflavone, (+)-N-3-benzylnirvanol, ketoconazole, 4-methylpyrazole hydrochloride, montelukast sodium, quinidine, sulfaphenazole, ticlopidine hydrochloride, and tranylcypromine sulfate), and NADPH regenerating system (glucose-6 phosphate dehydrogenase, glucose 6-phosphate, and NADP disodium salt). Sudoxicam (substrate), 5′-hydroxymethyl 5′-desmethyl meloxicam

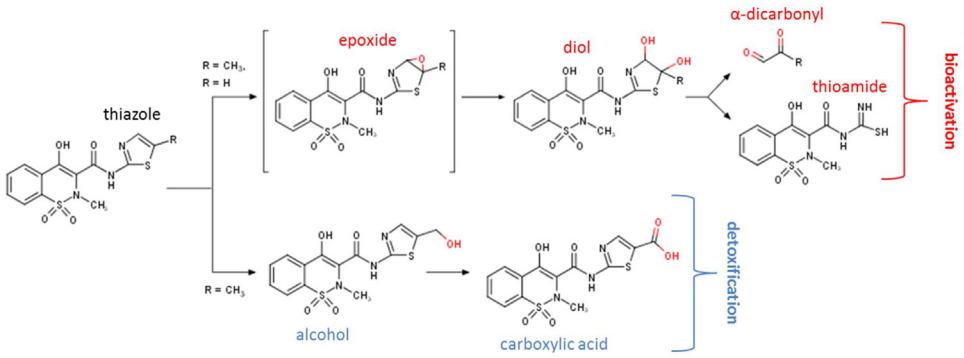

Scheme 1. Metabolic pathways for meloxicam and sudoxicam.

(metabolite standard), fluoxetine hydrochloride (internal standard), and 1,2-diamino-4,5-methylenedioxybenzene dihydrochloride (labeling agent) were obtained from Toronto Research Chemicals (Toronto, ON, Canada). Human liver microsomes pooled from 150 donors (HLM150) and recombinant enzyme Supersomes CYP1A2, 2A6, 2B6, 2C8, 2C9, 2C19, 2D6, 2E1, 3A4 and control prepared from baculovirus-transfected insect cells were purchased from Corning Gentest (Corning, NY).

2.2. Identification of P450s responsible for metabolism through inhibitor phenotyping

We identified P450 isozymes potentially contributing to sudoxicam and meloxicam bioactivation and detoxification pathways using selective chemical inhibitors in human liver microsomal reactions. Inhibitor choice and concentrations was based on literature showing selective bias or exclusivity in inhibiting specific isozymes: 1 mM 1-aminobenzotriazole (ABT) for general CYP activity (de Montellano, 2018), 16 μM α-naphthoflavone (ANF) for CYP1A2 (Spaggiari et al., 2014), 2 μM tranylcypromine (TCP) for CYP2A6, 3 μM ticlopidine (TIC) for CYP2B6 (Hartman et al., 2014; Khojasteh et al., 2011), 16 μM montelukast (MTK) for CYP2C8 (Tornio et al., 2006), 10 μM sulfaphenazole (SPA) for CYP2C9, 16 μM (+)-N-3-benzylnirvanol (BZV) for CYP2C19, 2 μM quinidine (QND) for CYP2D6, 30 μM 4-methylpyrazole (4-MP) for CYP2E1, and 1 μM ketoconazole (KCZ) for CYP3A4 (Hartman et al., 2014; Khojasteh et al., 2011; Nirogi et al., 2015). Each inhibitor was prepared in methanol and then diluted into phosphate buffer as a working solution. Methanol concentration was <0.1 % in the final reaction mixture, so cosolvent effect on enzyme activity was insignificant.

Reactions were conducted in 50 mM potassium phosphate buffer pH 7.4 and contained 10 μM sudoxicam or meloxicam, 0.5 mg/mL protein (HLM150), specific CYP inhibitors, and 0.1 % (final) DMSO co-solvent due to solubility limits of substrates. Reaction mixtures were pre-incubated for 15 min with 350 rpm shaking at 37 °C using a BMG Labtech THERMOstar incubator and then initiated with addition of NADPH regenerating system (final: 0.4 U/μL 1-glucose-6 phosphate dehydrogenase, 3.3 mM glucose 6-phosphate, 3.3 mM $MgCl_2$, 1.3 mM NADP+). Reactions lacking substrate served as negative controls for metabolite background signals. All reactions were incubated with shaking at 37 °C for 40 min and then quenched with a 2-fold volume of ice-cold methanol containing 200 μM fluoxetine or 10 μM hydroxycoumarin (internal standards for mass and fluorescence detection, respectively). Quenched reactions were incubated on ice for 5 min and then centrifuged for 15 min at 4 °C and 2500 rpm (2800 G) using a Beckman GPR centrifuge. The supernatant was transferred to a microplate and processed based on the method of analysis for α-dicarbonyl metabolites or 5-hydroxymethyl-meloxicam (*vide infra*). Reactions were conducted in triplicate and repeated two to four times. Background peaks were subtracted based on control reactions and resultant values normalized to reaction rates observed in absence of inhibitors to yield a percent activity value. Statistical differences of normalized rates from control were determined by Student's *t*-test (p-value 0.05).

2.3. Sudoxicam and meloxicam metabolism by recombinant P450s

We assessed directly the metabolic capacity of individual recombinant P450s. First, we conducted a screen of recombinant P450s to validate the inhibitor phenotyping studies for meloxicam and sudoxicam bioactivation. For reactions, 100 nM recombinant Supersomes for CYP1A2, 2A6, 2B6, 2C8, 2C9, 2C19, 2D6, 3A4, or 2E1 was pre-incubated with 400 μM substrate in 50 mM potassium phosphate buffer pH 7.4 (0.1 % volume DMSO) for 15 min at 37 °C with 350 rpm shaking using a BMG Labtech THERMOstar incubator. Reactions were initiated by addition of the NADPH regenerating system and incubated for 30 min at 37 °C with shaking. Reaction mixtures without substrate served as negative controls. All reactions were quenched and prepared as described in Section 2.2. All screening reactions were conducted in triplicate. Second, we carried out steady-state kinetic studies for P450s implicated in metabolism for sudoxicam and meloxicam. We initially identified conditions for linearity in reaction rates as a function of time and protein concentration. Those findings led to selection of actual protein concentration and reaction time for each isozyme. Aside from varying substrate concentrations, the remainder of reaction mixture and work up was identical to that described in Section 2.2. All reactions were conducted in triplicate with at least two replicates per substrate concentration.

2.4. Analysis of α-dicarbonyl metabolites from sudoxicam and meloxicam metabolism

Bioactivation of sudoxicam and meloxicam yields protoxin thioamide and an α-dicarbonyl cometabolite, *i.e.* glyoxal and methylglyoxal, respectively (Scheme 1). Due to thioamide reactivity, we measured kinetics for the α-dicarbonyl metabolites after trapping with fluorescent 1,2-diamino-4,5-methylenedioxybenzene (DMB) as described previously (Barnette et al., 2020). Briefly, dried reaction supernatants were resuspended in acetonitrile and combined with equal volume of water containing 1.0 M β-mercaptoethanol, 28 mM sodium hydrosulfite, and 7.0 mM DMB for a total reaction volume of 40 μL. Mixtures were sealed, incubated at 60 °C for 40 min, and quenched by diluting 20-fold in mobile phase for HPLC analysis (20 % acetonitrile, 80 % water + 0.1 % formic acid). Standard curves for glyoxal and methylglyoxal were prepared and labeled with the same procedure to quantitate metabolites. Prepared samples were analyzed with different gradient methods for labeled methylglyoxal and glyoxal using a 4.6 × 150 mm XSelect 3.5 μM HSS T3 column heated to 45 °C and a Waters Acquity Arc UPLC equipped with QDa (MS) and fluorescence detectors (Milford, MA). Labeled glyoxal and methylglyoxal were resolved with similar published gradient methods (Barnette et al., 2020) using mobile phase containing 0.1 % formic acid/water and 0.1 % formic acid/acetonitrile. Resolved samples were monitored by fluorescence (excitation: 325 nm; emission: 393 nm), and peak areas normalized to internal standard (7-hydroxycoumarin) and corrected for background responses using peak areas from control reactions without substrate. Serial dilution standard curves were used to convert the resultant values to analyte quantities. Rate calculations and kinetic analyses were carried out as described in Section 2.6.

2.5. Analysis of 5-hydroxymethyl-meloxicam from meloxicam metabolism

Meloxicam metabolism includes a detoxification pathway yielding 5-hydroxymethyl-meloxicam (Scheme 1). For these kinetic studies, dried reaction supernatants were resuspended directly in mobile phase (20 % acetonitrile, 80 % water + 0.1 % formic acid) for HPLC-MS analysis using an authentic 5-hydroxymethyl-meloxicam standard (368 *m/z*). As described previously (Barnette et al., 2020), metabolites were resolved chromatographically with a gradient of 0.1 % formic acid/water and 0.1 % formic acid/acetonitrile using a Cortecs C-18 2.7 μm column (4.6 × 50 mm) on a Waters Acquity Arc UPLC system equipped with a QDa (MS) detector (Milford, MA). QDa cone voltage was 20 V to detect *m/z* signals from a range of 150–650 in positive ion mode. Analyte peak areas were normalized to internal standard (fluoxetine, *m/z* 310).

Rate calculations and kinetic analyses were carried out as described in Section 2.6.

2.6. Modeling metabolic kinetics for sudoxicam and meloxicam

From reaction data, we calculated the kinetics and extrapolated their potential relevance in hepatic clearance based on relative P450 levels. First, we calculated initial rates (pmol/min/nmol protein) for metabolite levels as a function of time and plotted rates against substrate concentration. Resultant kinetic profiles were fit to Michaelis-Menten, biphasic or allosteric models and the best fit determined based on the extra sum-of-squares F test using GraphPad Prism 7.0 (GraphPad Software, Inc; San Diego, CA). Next, we extrapolated *in vitro* kinetics to *in vivo* detoxification and bioactivation of sudoxicam and meloxicam using an approach described in our previous publication (Barnette et al., 2019). In brief, we used reported average protein concentrations (Yu and Haining, 2001) from quantitative MS analysis of 11 P450s present in human liver microsomes pooled from 610 donors (Kawakami et al., 2011) to calculate scaled values by multiplying kinetic efficiencies (V_{max}/K_m) for each P450 by respective fractional concentrations (Equation 1). Percent contributions were calculated by dividing the scaled values by the sum of scaled values for all contributing P450s in the pathway (Equation 2).

Equation 1:

$$Scaled\ \ P450\ \ contribution = \frac{Vmax}{Km} * \frac{[isozyme]}{[total\ \ protein]}$$

Equation 2:

$$P450 \quad \% \quad contribution = \frac{\frac{Vmax}{Km} * \frac{[isozyme]}{[total \quad protein]}}{Total \quad P450 \quad contributions} * 100\%$$

2.7. Seeking patterns for meloxicam-dependent liver injury

We used two methods and data sources to conduct an exploratory search for possible drug-drug interactions correlating with meloxicam-associated liver toxicity that could be explained by findings from our bioactivation studies. First, we accessed the publicly available FDA Adverse Events Reporting System (FAERS) using the FAERS Public Dashboard ("FDA Adverse Event Reporting System (FAERS) Public Dashboard," 2020) and searched for all cases involving meloxicam from 1998 to 2020. We filtered results for hepatobiliary disorders and exported data to count and assess frequencies of concomitant products reported for applicable cases. Second, we conducted an informatics approach to mine electronic health records from the BJC HealthCare network at St. Louis. For effective data analysis, we proposed a simple, innovative deep learning model that estimated meloxicam-dependent risk of drugs on DILI. Our model architecture took each hospitalizations' drugs as input where each hospitalization $V \in R^{|C|}$, where C was equal to 1083, was represented as the sum of one-hot vectors. The one-hot vectors were binary vectors of dimension |C| where each bit represented a specific drug. A bit was set to 1 if a specific drug was present, otherwise 0 if absent. This higher dimensional representation of drugs helped us encode more meaningful information and train the model. The model architecture consisted of an interaction network, wherein the drug vector input was multiplied (element-wise) by a binary scalar variable that represented if meloxicam was prescribed to the hospitalizations (Fig. 1). Thus, for hospitalizations which were not prescribed meloxicam, the interaction network output was zero. This clinical deep learning model will be published in a separate study.

3. Results

3.1. CYP2C8, 2C19, and 3A4 bioactivated sudoxicam with varying efficiencies

We used a two-tiered system to identify which P450s were responsible for sudoxicam bioactivation as measured previously by glyoxal formation (Scheme 1) using human liver microsomes (Barnette et al., 2020; Obach et al., 2008). Our initial screen of microsomal sudoxicam bioactivation involved selective chemical inhibitors for P450s. Reactions incubated with nonspecific P450 inhibitor ABT resulted in 75 % inhibition of glyoxal formation, indicating a major role for P450 activity. Based on targeted P450 inhibition, statistically significant decreases in glyoxal formation implicated contributions by CYP2B6, 2C8, 2C19, 2D6, and 2E1 (Fig. 2A). Surprisingly, the CYP1A2 inhibitor ANF actually increased significantly the extent of the reaction. Second, we conducted subsequent validation studies with recombinant P450s and revealed only CYP2C8, 2C19, and 3A4 were capable of catalyzing the reaction (Fig. 3A). These results confirmed contributions from CYP2C8 and 2C19 and revealed metabolism by CYP3A4 when compared to inhibitor phenotyping experiments.

Based on direct evidence from recombinant P450s, we further characterized sudoxicam bioactivation by CY2C8, 2C19, and 3A4. As a first step, we identified steady-state conditions for sudoxicam bioactivation by CYP2C8, 2C19, and 3A4 by establishing linearity of glyoxal formation over reaction time and enzyme concentration (Supporting Information S1, S2). Optimized reactions were then

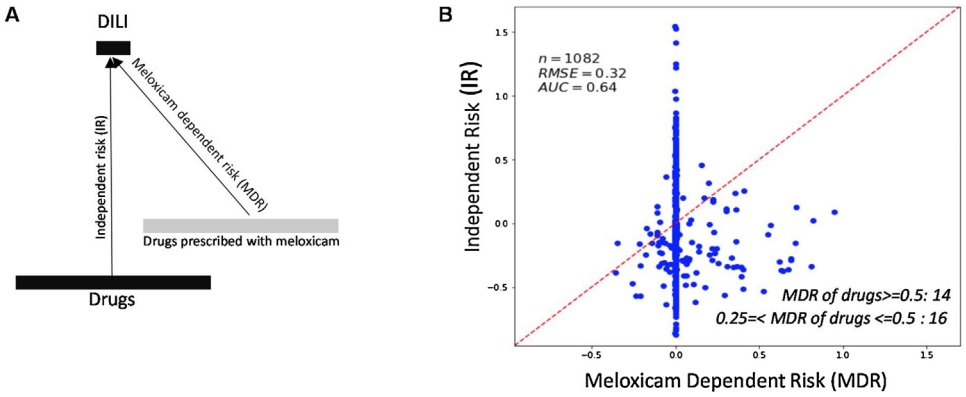

Fig. 1. Clinical cohort analysis using deep learning model. (A.) The Neural Network architecture to simultaneously capture independent risk (IR) and Meloxicam dependent risk (MDR) is a feedforward neural network that aims to predict drug induced liver injury (DILI) using independent occurrence of drugs and drugs that occur alongside meloxicam among hospitalized patients. (B.) Independent risk (IR) for drugs was plotted as a function of Meloxicam dependent risk (MDR). The cluster of points along the axis MDR = 0.0 shows that most drugs do not exhibit a meloxicam dependent response.

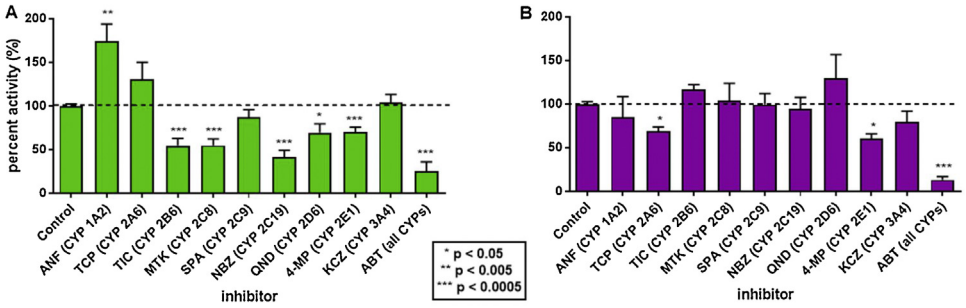

Fig. 2. Inhibitor phenotyping of sudoxicam and meloxicam bioactivation. (A.) 10 μM sudoxicam (green) and (B.) 10 μM meloxicam (purple) were incubated in HLM with and without P450 specific inhibitors to measure alpha-dicarbonyl metabolite levels. Inhibitors used were 1-aminobenzotriazole (ABT) for general P450 activity, α-naphthoflavone (ANF) for CYP1A2, tranylcypromine (TCP) for CYP2A6, ticlopidine (TIC) for CYP2B6, montelukast (MTK) for CYP2C8, sulfaphenazole (SPA) for CYP2C9, (+)-N-3-benzylnirvanol (BZV) for CYP2C19, quinidine (QND) for CYP2D6, 4-methylpyrazole (4-MP) for CYP2E1, and ketoconazole (KCZ) for CYP3A4. Significant differences were determined using Student's T test ($p < 0.05$). Reactions were replicated 3-6 times per inhibitor. Error bars denote standard error.

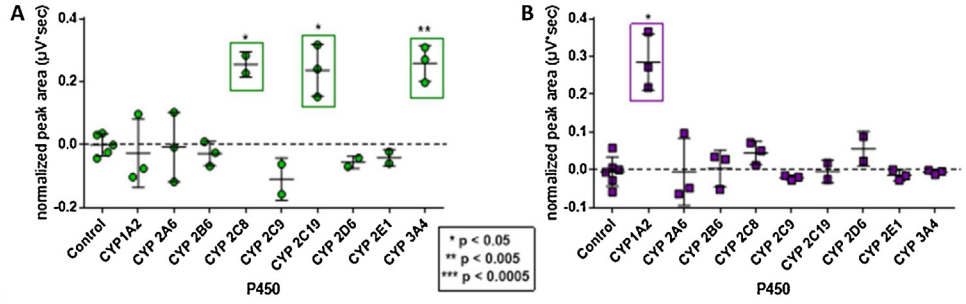

Fig. 3. Recombinant P450 screen for sudoxicam and meloxicam bioactivation. (A.) 400 μM sudoxicam and (B.) 400 μM meloxicam were incubated with recombinant P450s to measure glyoxal (green circles) and methylglyoxal (purple squares) formation. Significant differences from background (dashed line) were determined based on $p < 0.05$ calculated using Student's t test. Error bars denote standard error.

carried out at 10 nM CYP3A4, 2C8, and 2C19 for 40 min to measure initial rates as a function of substrate concentration. For all P450s, the kinetic profiles yielded data that fit best to a Michaelis-Menten model (Fig. 4A). CYP2C19 demonstrated the highest V_{max}, which was two-fold greater than that of CYP2C8 and four-fold more than CYP3A4 (Table 1). K_m values for CYP2C19 and 3A4 were comparable; however, CYP2C8 had a much higher affinity for sudoxicam based on a five-fold lower K_m. Taken together, CYP2C8 was more than two-fold more efficient at sudoxicam bioactivation compared to the other P450s.

3.2. Only CYP1A2 bioactivated meloxicam

Similarly, we used a two-tiered system to identify P450s contributing to meloxicam bioactivation as measured by formation of methylglyoxal (Scheme 1). The general P450 inhibitor ABT blocked 85 % of the reaction with human liver microsomes, confirming their role in meloxicam bioactivation (Barnette et al., 2020), and reactions with selective inhibitors implicated CYP2A6 and 2E1 (Fig. 2B); however, neither P450 formed methylglyoxal in our follow-up recombinant enzyme screen. Instead, CYP1A2 was

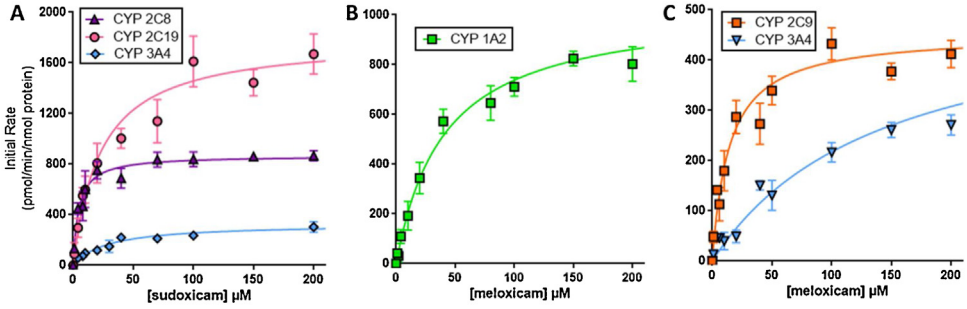

Fig. 4. Steady state kinetic profiles for sudoxicam and meloxicam metabolic pathways in recombinant P450 isozymes. (A.) Sudoxicam bioactivation rates (glyoxal) were measured in recombinant CYP2C8 (purple triangles), CYP2C19 (pink circles), and CYP3A4 (blue diamonds). (B.) Meloxicam bioactivation rates (methylglyoxal) were measured in recombinant CYP1A2 (green squares). (C.) Meloxicam detoxification rates (5-hydroxymethyl-meloxicam) were measured in recombinant CYP2C9 (orange squares) and CYP 3A4 (blue triangles). Reactions for each substrate concentration were replicated 6-9 times. Kinetics fit best to the Michaelis-Menten equation. Reaction efficiencies (V/K) were calculated using V_{max} and K_m. Units: V_{max}: pmol/min/ mg enzyme, K_m: μM.

Table 1
Michaelis-Menten Kinetic Constants for Sudoxicam and Meloxicam Metabolites from Recombinant CYP Isozymes.

	Steady-state kinetic constants for individual metabolites[a]				
P450 Isozyme	Substrate	Metabolite	V_{max}[b]	K_m (μM)	V_{max}/K_m
CYP1A2	sudoxicam	glyoxal			
	meloxicam	methylglyoxal	1000 ± 53	40 ± 7.5	**25**
		5-hydroxymethyl-meloxicam			
CYP2C8	sudoxicam	glyoxal	870 ± 30	4.6 ± 0.89	**190**
	meloxicam	methylglyoxal			
		5-hydroxymethyl-meloxicam			
CYP2C9	sudoxicam	glyoxal			
	meloxicam	methylglyoxal			
		5-hydroxymethyl-meloxicam	450 ± 15	14 ± 2.5	**32**
CYP2C19	sudoxicam	glyoxal	1800 ± 120	23 ± 5.2	**78**
	meloxicam	methylglyoxal			
		5-hydroxymethyl-meloxicam			
CYP3A4	sudoxicam	glyoxal	330 ± 17	29 ± 5.8	**11**
	meloxicam	methylglyoxal			
		5-hydroxymethyl-meloxicam	530 ± 54	140 ± 38	**3.8**

[a] Best fit models shown in Fig. 5 were determined using corrected Akaike information criterion. Values shown with standard error from mean.
[b] Units are pmol/min/nmol protein.

the only recombinant P450 to form detectable levels of methylglyoxal (Fig. 3B). Based on those results, we focused kinetic studies on CYP1A2-mediated bioactivation of meloxicam. From control experiments (Supporting Information S1, S2), we identified steady-state conditions for reactions to be 25 nM CYP1A2 for a 40 min reaction. The kinetic profile for CYP1A2 bioactivation of meloxicam was best described by the Michaelis-Menten model (Fig. 4B). The V_{max} was comparable to that for sudoxicam bioactivation by CYP2C8; however, the ten-fold higher K_m indicated a relatively low affinity of meloxicam for CYP1A2. Thus, the overall efficiency for meloxicam bioactivation was seven-fold lower than that observed for the dominant sudoxicam bioactivation P450 (Table 1).

3.3. CYP2C9 and 3A4 detoxified meloxicam through 5-hydroxylation of the methyl group

The relative significance of meloxicam bioactivation will depend on the competing detoxification pathway involving oxidation of its methyl group to form 5-hydroxymethyl-meloxicam under the same reaction conditions. This alternate pathway was attributed solely to CYP2C9 and 3A4 in previous studies (Chesne et al., 1998) and thus, we replicated those steady-state kinetic studies with slight variations in our case such as minimizing co-solvent use and holding the amount constant in experiments. Our control experiments revealed that 25 nM CYP2C9 and 3A4 for meloxicam hydroxylation for 40 min reactions were optimal for steady-state studies (Supporting Information S1, S2). For both P450s, analysis of kinetic profiles favored the Michaelis-Menten model to describe the data (Fig. 4C). V_{max} values were comparable between the two enzymes, but CYP2C9 had a much higher affinity for meloxicam based on the respective K_m values. The net effect was an approximate ten-fold higher efficiency of CYP2C9 hydroxylation of the meloxicam methyl group relative to CYP3A4 (Table 1).

3.4. P450 levels mitigated extrapolated relevance of P450 bioactivation and detoxification

Under biological conditions in the liver, relative contributions of individual P450s to meloxicam bioactivation and detoxification pathways depend on two factors: (1) relative P450 efficiencies to catalyze pathways and (2) relative P450 abundance in the liver. Based on clinical studies (Gschwend et al., 2007), we assumed drug levels were below K_m (subsaturating), so that metabolic flux rates would depend linearly on V_{max}/K_m. We scaled metabolic fluxes using average P450 concentrations reported by others using MS analysis of 610 pooled human liver microsomes (Kawakami et al., 2011). We then calculated the potential *in vivo* relevance of P450s in drug bioactivation and detoxification to assess the magnitude of metabolic flux down each pathway (Equation 1) and P450 contributions within the pathways (Equation 2). Efficiency values were normalized per mg protein as described previously (Barnette et al., 2020) (Table 2). Summation of P450 contributions to sudoxicam bioactivation showed metabolic flux down the pathway to be 14-fold the magnitude of flux down the meloxicam bioactivation pathway. Overall flux for meloxicam detoxification was six-fold that of the competing bioactivation pathway, which contrasts with the less than two-fold difference based solely on P450 efficiency. For analysis of P450 relative contributions within each pathway, we expressed results as percentages of total isozyme contribution per pathway (Table 3, Fig. 5). Due to high metabolic efficiency, CYP2C8 was the dominant P450 responsible for sudoxicam bioactivation relative to CYP2C19 and 3A4, even though the latter two P450 s are far more abundant in the liver. For meloxicam, there is no similar comparison, because CYP1A2 was the only P450 involved in bioactivation. The detoxification pathway for meloxicam was primarily due to CYP2C9 activity with minor contributions from CYP3A4. The extrapolated potential

Table 2
Scaled contributions of P450 isozymes to *in vivo* hepatic sudoxicam and meloxicam clearance and/or bioactivation.

Substrate	Metabolite	Scaled contributions[a] of individual isozymes for each reaction[b]					
		CYP1A2	CYP2C8	CYP2C9	CYP2C19	CYP3A4	Total
sudoxicam	glyoxal	–	5.54	–	0.285	0.736	6.55
meloxicam	methylglyoxal	0.457	–	–	–	–	0.457
	5-hydroxy-methyl-meloxicam	–	–	2.56	–	0.234	2.79

[a] Units: V_{max}/K_m = pmol/min/mg protein/μM substrate.
[b] Calculations based on extrapolations of kinetic efficiencies and reported levels of P450 isozymes (pmol/mg protein) as described under Materials and Methods.

Table 3
Relative contributions of P450 isozymes to *in vivo* hepatic sudoxicam and meloxicam clearance and/or bioactivation.

Substrate	Metabolite	Percent contributions of individual isozymes for each reaction[a]				
		CYP1A2	CYP2C8	CYP2C9	CYP2C19	CYP3A4
sudoxicam	glyoxal	–	84.4	–	4.3	11.2
meloxicam	methylglyoxal	100	–	–	–	–
	5-hydroxymethyl-meloxicam	–	–	91.6	–	8.4

[a] Calculations based on extrapolations of kinetic efficiencies and reported levels of P450 isozymes as described under Materials and Methods.

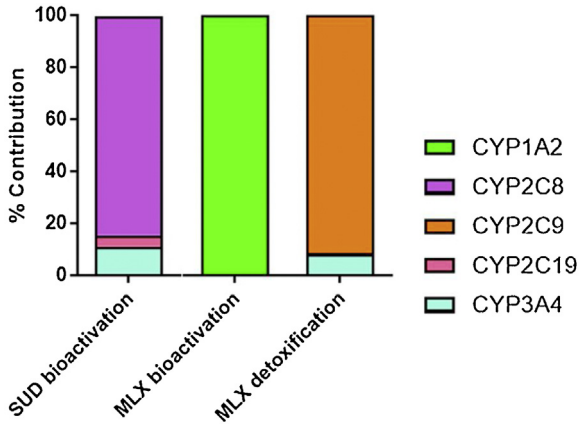

Fig. 5. *In vitro* to *in vivo* extrapolation of P450 pathway contributions. Efficiencies for sudoxicam and meloxicam bioactivation and meloxicam detoxification by P450 isozymes were scaled to model their relative contributions in the average human liver based on average P450 concentrations. P450 contributions are shown as percentages of the total P450 activity along each pathway.

P450 roles in bioactivation and detoxification are summarized visually in Scheme 2.

3.5. Exploratory search of FAERS database revealed possible drug-drug interactions

We used the publicly available FDA Adverse Events Reporting System (FAERS) to conduct an exploratory search for possible drug-drug interactions correlating with meloxicam-associated liver toxicity that could be explained by our bioactivation findings. We identified 326 total cases of hepatobiliary disorders involving meloxicam use from 1998 to 2020 with 308 cases being serious and 39 resulting in death. From these cases, we found a total of 354 reported co-administered products with meloxicam. The most frequent co-administered drug was omeprazole, (21 cases) and lansoprazole was second (18 cases). These proton pump inhibitors are then possible perpetrators of drug-drug interactions with meloxicam.

3.6. Clinical cohort for electronic health record mining contained meloxicam patients

The BJC HealthCare network at St. Louis houses an electronic health record database of 397,064 hospitalizations. The cohort includes 176,443 (44.44 %) male hospitalizations, 189,723 (47.78 %) female hospitalizations and 30,878 (7.77 %) hospitalizations that had no information on gender. The cohort contains hospitalizations with a median age of 63.2 years and median hospitalization stay of 3 days. The median number of drugs prescribed was 13 (max: 101; min: 1). Each hospitalization included diagnoses (23366 ICD 9,10 codes), drugs (1083 unique active ingredients) and procedures (13097 ICD 9-CM, 10-PCS codes). In this study, we included drugs that were administered orally or *via* intravenous injection or infusion. In the patient cohort, we found that meloxicam was prescribed to 4570 hospitalizations. We combined diagnosis codes, procedure codes and laboratory results (namely, alkaline phosphatase, alanine aminotransferase, aspartate aminotransferase and bilirubin levels) to identify 2800 hospitalizations as reflective of DILI. Among those hospitalizations, we identified 8 that had been prescribed meloxicam. No comparable data exists for sudoxicam given that it never made it to market.

3.7. Clinical cohort analysis identified drugs possibly linked with meloxicam-induced liver injury

Clinical deep learning models (section 2.7) were trained on the BJC patient cohort data to estimate both independent risk (IR) and meloxicam dependent risk (MDR) of a drug. Trained models differed in how the DILI target variable was defined.

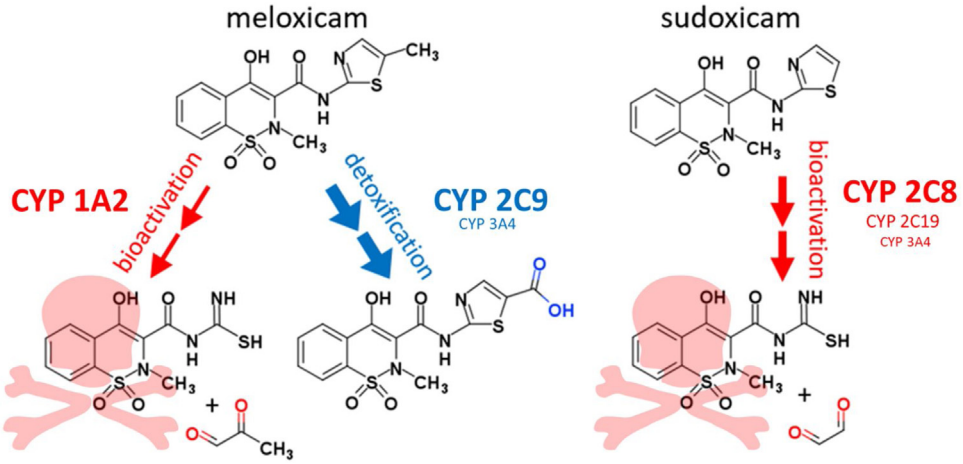

Scheme 2. P450 isozymes participating in thiazole bioactivation and detoxification pathways.

Hospitalizations were treated as DILI positive based on the diagnostic and procedure codes along with the absence or inclusion of elevated liver enzyme measures such as alanine aminotransferase (ALT) and aspartate aminotransferase (AST). We used the weights that link the input vectors to the DILI hospitalization target as proxies for IR and MDR. Weights were learned by the model and the higher the weight, the higher the association of that input to predicting the DILI hospitalization target. Both trained models were evaluated on the BJC patient cohort described in section 3.6 and the IR and MDR were computed for 1083 unique active ingredients. Significance values for the model MDR predictions were computed using Fisher's exact test ($p < 0.05$). In enumerating drugs with significant MDR elevation relative to IR, we considered only those drugs that achieved an MDR of at least 0.30. Across the drugs evaluated, 11 had significant MDR values with respect to the diagnostic and procedure codes DILI model and 7 had significant MDR values with respect to the diagnostic codes, procedure codes, and liver enzymes DILI model, yet only one drug was significant in both DILI models. All drugs that at least one of the clinical deep learning models designated with significant MDR value are recorded in Supporting Information S3. Drugs were annotated whether they were known CYP1A2 inducers or CYP2C9/3A4 inhibitors.

4. Discussion

4.1. Meloxicam methyl group altered P450-specific thiazole bioactivation versus *sudoxicam*

Based on human liver microsomal kinetics, introduction of a methyl group reduced efficiency of thiazole bioactivation 6-fold for meloxicam relative to sudoxicam (Barnette et al., 2020). Nevertheless, this significant effect was not due to a simple alteration in binding and chemistry but P450 selectivity for specific reactions. Initial inhibitor phenotyping studies implicated many P450s involved in drug bioactivations and an unexpected increase in sudoxicam bioactivation with the CYP1A2 inhibitor α-naphthoflavone. The latter effect was likely due to allosteric CYP3A4 activation (Woods et al., 2011) and serves as a cautionary reminder of potential artifactual observations when using chemical inhibitors. For validation, we screened metabolism by recombinant P450s, which demonstrated roles for CYP2C8, 2C19, and 3A4 in sudoxicam bioactivation and only CYP1A2 for meloxicam bioactivation. Incomplete inhibition by ABT of CYP1A2 for meloxicam and CYP2C8 and 2C19 for sudoxicam microsomal reactions (Linder et al., 2009) likely explains observed residual activity for the bioactivation pathways of both drugs when preincubated with ABT (Barnette et al., 2020). Direct bioactivation evidence from recombinant P450 reactions then justified our subsequent focus on characterizing their reaction kinetics for sudoxicam and meloxicam.

4.2. Insect hydrolases may contribute to bioactivation pathways by recombinant P450s

Recombinant P450s Supersomes provide a convenient tool for assessing sudoxicam and meloxicam metabolism by individual P450s, yet thiazole bioactivation involves multiple steps, including P450-mediated oxidation and subsequent cleavage of the epoxide (Scheme 2). Based on our previous studies, sudoxicam, and not meloxicam, bioactivation required human microsomal epoxide hydrolase (mEH) activity (Barnette et al., 2020). The mEH inhibitor elaidamide blocked eventual formation of glyoxal from sudoxicam metabolism. For current recombinant P450 studies, Supersomes lack human mEH, yet sudoxicam reactions yielded glyoxal anyway, suggesting presence of endogenous insect epoxide hydrolase(s). As possible evidence, an epoxide hydrolase from *Anopheles gambiae* displays activity toward xenobiotic molecules like drugs. Moreover, this enzyme shares homology with a mammalian epoxide hydrolase isoform (Xu et al., 2014) making a role in the sudoxicam bioactivation pathway plausible for an analogous enzyme present in Supersomes. To our knowledge, there are no known inhibitors for insect epoxide hydrolases to explore this possibility; however, its occurrence warrants consideration, when carrying out and analyzing recombinant P450 kinetics prepared with insect cells.

4.3. P450 bioactivation kinetics explained findings for microsomal reactions

Despite differences in composition, recombinant P450s are useful reagents to assess and extrapolate kinetics determined with human liver microsomes. From our previous studies, microsomal sudoxicam bioactivation exhibited a multi-phasic kinetic curve that was best modeled by a saturable Michaelis-Menten mechanism followed by an unsaturable linear phase (Barnette et al., 2020). Rather than cooperative metabolism by a single P450 (Atkins, 2005; Denisov et al., 2009), the non-hyperbolic kinetics reflected collective contributions from three different P450s based on our screening and kinetic studies. The more efficient Michaelis-Menten phase for the microsomal kinetic profile reflected likely CYP2C8 due to comparable K_m values, *i.e.* 6, *versus* 5 μM respectively. The K_m values for CYP2C19 and 3A4 were at least five-fold higher and thus would be reflected in the less saturable phase of sudoxicam bioactivation. By contrast, microsomal meloxicam bioactivation conformed to Michaelis-Menten kinetics, suggesting catalysis by a single isozyme. Similarity of K_m values for microsomal and recombinant CYP1A2 kinetic profiles (26 *vs* 40 μM) provides reasonable support for the sole role of CYP1A2 in meloxicam bioactivation.

4.4. Steady-state meloxicam detoxification was mainly by CYP2C9 with minor 3A4 role

Previous studies by Chesne et al. ascribed roles for CYP2C9 and 3A4 in meloxicam hydroxylation and subsequent detoxification (Chesne et al., 1998). Use of high and varying levels of DMSO in their studies could have impacted reported kinetic mechanisms and constants (Chauret et al., 1998; Easterbrook et al., 2001), and thus, we carried out those studies conforming to our experimental design. For CYP2C9, we observed the same mechanism and comparable K_m (14 *versus* 9.6 μM), as determined previously. By contrast, we measured a significant three-fold lower K_m for the CYP3A4 reaction. The mid-point of the kinetic profile was at 140 μM as opposed to the previously reported 475 μM. The most likely source for this discrepancy is experimental design. Of P450s, CYP3A4 is the most DMSO sensitive, showing inhibition at DMSO concentrations as low as 0.2 % (Chauret et al., 1998), and Chesne et al. used a concentration range from 1 to 0.1 %. In our study, we used a low constant DMSO concentration (0.1 %), which was established previously using control experiments to identify a minimal cosolvent concentration necessary to achieve substrate solubility (Barnette et al., 2020). This condition limited substrate concentrations for our assays, while providing higher accuracy by minimizing DMSO impact on P450 activities (Chauret et al., 1998; Easterbrook et al., 2001). Contributions from CYP2C9 and 3A4 could explain our previously reported biphasic microsomal kinetic profile for meloxicam hydroxylation (Barnette et al., 2020). The kinetic profile fit best to a saturable Michaelis-Menten mechanism with an unsaturable linear phase. The more efficient Michaelis-Menten phase yielded a K_m of 15 μM, which is nearly identical to the 14 μM K_m for recombinant CYP2C9 reaction. The less efficient

linear phase of the microsomal profile reflects likely the contribution from the ten-fold less efficient CYP3A4. Taken together, there is excellent agreement between our recombinant CYP2C9 and 3A4 kinetic data and that reported for human liver microsomes.

4.5. In vitro *to* in vivo *extrapolation revealed individual P450s dominated bioactivation and detoxification*

Metabolic flux of drugs down bioactivation pathways depends on reaction kinetics and protein concentration, and thus we used our current findings with *in vitro* studies to extrapolate *in vivo* P450 contributions for each pathway when taking hepatic P450 levels into account. For meloxicam metabolism, all contributing P450 K_ms were at least 14 μM, which is over four-fold greater than reported maximum plasma levels for the drug in patients (3.2 μM) (Gschwend et al., 2007) indicating sub-saturating metabolic conditions. Consequently, relative P450 contributions to metabolism can accurately be estimated based on efficiencies (V_{max}/K_m). Due to toxicity, sudoxicam never made it to clinic, so we assumed similar drug levels in patients as reported for meloxicam and thus, sub-saturating conditions for calculations. These extrapolations allowed us to assess P450 concentration impacts on metabolic flux and compare findings from liver metabolism modeled by recombinant P450 kinetics to those reported using pooled human liver microsomes (Barnette et al., 2020). For meloxicam, combined scaled P450 values were very similar to microsomal efficiencies for bioactivation (0.45 *vs* 0.32) and detoxification (2.8 *vs* 1.9), with both sets of data showing 6-fold higher flux for detoxification. For sudoxicam, combined P450 values were three-fold the calculated efficiency in microsomal reactions, which may be partially explained from exclusion of the low-affinity microsomal kinetic phase in the extrapolation calculations. Our assessment of P450 contributions showed that each pathway was dominated by at least 80 % contribution from an individual P450. Sudoxicam bioactivation was dominated by CYP2C8 while meloxicam bioactivation was exclusively catalyzed by CYP1A2, and meloxicam detoxification was dominated by CYP2C9. Importantly, extrapolation models reflect an “average” metabolic capacity and not factors altering P450 concentrations and/or activities in patients. For meloxicam, clinical relevance of CYP1A2 and 2C9 would then depend on how factors like age, sex, race, genetic polymorphisms, state of health and drug-drug interactions modulate their relative activities toward bioactivation and detoxification.

4.6. Implication and investigation of drug-drug interaction patterns correlating with meloxicam toxicity

Co-administered drugs and lifestyle choices with meloxicam can increase or decrease CYP1A2 (Koonrungsesomboon et al., 2017; Horn and Hansten, 2011a) and 2C9 (Booven et al., 2011; Horn and Hansten, 2011b) activities and, hence, modulate drug bioactivation and associated toxicological outcomes. Cigarette smoking substantially increases CYP1A2 activity along with drugs including barbiturates, carbamazepine, primidone, and rifampin (Horn and Hansten, 2011a). Alternatively, drugs can inhibit CYP2C9 activity, notably amiodarone, fluconazole, and sulfaphenazole (Booven et al., 2011). There is currently no clinical evidence of drugs significantly interacting with meloxicam. We conducted an exploratory investigation for possible drug-drug interactions correlating with meloxicam-associated liver toxicity using data from the FDA Adverse Events Reporting System (FAERS) as part of a voluntary post-marketing drug safety surveillance program. Our search of hepatobiliary cases involving meloxicam use identified omeprazole and lansoprazole as the two most frequent concomitant drugs, each reported in 6% of the total applicable cases from 1998 to 2020. These drugs are proton pump inhibitors known to induce drug-drug interactions by altering P450 activities. Omeprazole induces CYP1A2 (Daujat et al., 1992) and inhibits 3A (Shirasaka et al., 2013). This drug could simultaneously increase meloxicam bioactivation while, to a lesser extent, decreasing its detoxification, and thus increase overall risk for hepatoxicity. Similarly, lansoprazole induces CYP1A2 and presumably increases toxic risk due to meloxicam bioactivation (Krusekopf et al., 2003). While these observations are consistent with our metabolic studies, they are not sufficient evidence of causality. Because submission of reports to FAERS is voluntary, there are limitations to using the system. It contains reports that lack verification or established causation and some reports are duplicated or incomplete. Due to these shortcomings, FAERS is not a reliable indicator of drug toxicity profiles and thus, other explanations are possible for the high frequencies of these drugs in the targeted cases. For example, it is unknown if these frequencies differ significantly from meloxicam patients not suffering from hepatobiliary cases, which are not represented in the data. It is possible that the proton pump inhibitors are commonly taken with meloxicam to alleviate its gastrointestinal side effects. Deeper analytical methods and more complete data sources are needed to investigate these possibilities; however, the easily accessible database was useful for our exploratory investigations to identify consistent patterns of drug coadministration that correlate with liver injury.

As an informatics approach, we sought to identify patterns in clinical health records from the BJC HealthCare network wherein drug interactions with meloxicam were associated with indications of liver injury depending on its classification. Of the drugs identified to significantly increase meloxicam-dependent liver injury ($p < 0.05$) based solely on diagnostic and procedure codes to infer DILI hospitalizations, only the CYP3A4 inhibitor esomeprazole is known to affect a meloxicam metabolizing P450. The addition of elevated liver enzymes to infer DILI hospitalizations identified no drugs with known CYP1A2 inducing or CYP2C9 or 3A4 inhibiting activity marked with significant elevation of meloxicam-dependent liver injury. The inability to identify more possible trends may reflect a limited positive liver injury training set ($n = 8$). This small set was expected given that meloxicam induced liver injury is rare and clinical protocols are in place to avoid liver injury (“Mobic [label],” 2000). A controlled clinical study is likely necessary to better address these possibilities. Nevertheless, based on the preliminary findings, this informatics and modeling approach holds promise with larger sample sizes. In addition, a more rigorous analysis of electronic health records is required to fully investigate the complexity of factors that could impact P450 activity in relation to hepatic toxicity; however, such an investigation is beyond the scope of this study.

4.7. Concluding remarks

Surprisingly, the addition of a simple methyl group on the sudoxicam scaffold impacts the bioactivation pathway by altering not only P450 affinity with the drug but also which P450 isozymes interact with the drug to catalyze the reactions. This revelation was possible due to our robust, quantitative kinetic approach to scale the impact of the difference in structure on metabolism. The dominance of individual, but different, P450s on bioactivation and detoxification pathways provides a tractable basis for predicting how alterations in those P450 activities could impact the relative significance of bioactivation and hence, toxic risks. Our exploratory informatics and modeling efforts provided preliminary evidence supporting

a possible link between our *in vitro* observations and possible liver injuries in the clinic that requires further study. Taken together, the significant impact of the methyl group on thiazole metabolism highlights the challenge in predicting the effects of even the simplest changes to molecular structure on the relative importance of bioactivations.

Funding

This work was supported by the National Library of Medicine of the National Institutes of Health [grant numbers R01LM012222, R01LM012482]; the National Institute of General Medical Sciences [grant number T32GM106999]; National Institutes of Health (NIH) NCRR [grant numbers 1S10RR022984-01A1, 1S10OD018091-01]; and the University of Arkansas for Medical Science Vice Chancellor of Research Equipment Grant.

Declaration of Competing Interest

The authors report no declarations of interest.

Appendix A. Supplementary data

Supplementary material related to this article can be found, in the online version, at doi:https://doi.org/10.1016/j.toxlet.2020.11.015.

References

Ahmed, M., Khanna, D., Furst, D.E., 2005. Meloxicam in rheumatoid arthritis. Expert Opin. Drug Metab. Toxicol. 1, 739–751.
Atkins, W.M., 2005. Non-michaelis-menten kinetics in cytochrome P450-catalyzed reactions. Annu. Rev. Pharmacol. Toxicol. 45, 291–310. doi:http://dx.doi.org/10.1146/annurev.pharmtox.45.120403.100004.
Ayati, A., Emami, S., Asadipour, A., Sha, A., Foroumadi, A., 2015. Recent applications of 1, 3-thiazole core structure in the identification of new lead compounds and drug discovery. Eur. J. Endocrinol. 97, 699–718. doi:http://dx.doi.org/10.1016/j.ejmech.2015.04.015.
Barnette, D.A., Davis, M.A., Flynn, N., Pidugu, A.S., Swamidass, S.J., Miller, G.P., 2019. Comprehensive kinetic and modeling analyses revealed CYP2C9 and 3A4 determine terbinafine metabolic clearance and bioactivation. Biochem. Pharmacol. 170.
Barnette, D.A., Schleiff, M.A., Osborn, L.R., Flynn, N., Matlock, M., Swamidass, S.J., 2020. Dual mechanisms suppress meloxicam bioactivation relative to sudoxicam. Toxicology 440.
Booven, D.V., Marsh, S., McLeod, H., Carrillo, M.W., SangKuhl, K., Klein, T.E., Altman, R.B., 2011. Cytochrome P450 2C9-CYP2C9. Pharmacogenet. Genomics 20, 277–281. doi:http://dx.doi.org/10.1097/FPC.0b013e3283349e84.
Chauret, N., Gauthier, A., Nicoll-griffith, D.A., 1998. Accelerated communication: effect of common organic solvents on in vitro cytochrome p450-mediated metabolic activities in human liver microsomes. Drug Metab. Dispos. 26, 4–7.
Chesne, C., Guyomard, C., Guillouzo, A., Schmid, J., Ludwig, E., Sauter, T., 1998. Metabolism of meloxicam in human liver involves cytochromes P4502C9 and 3A4. Xenobiotica 28, 1–13.
Dalvie, D.K., Kalgutkar, A.S., Khojasteh-bakht, S.C., Obach, R.S., Donnell, J.P.O., 2002. Biotransformation reactions of five-membered aromatic heterocyclic rings. Chem. Res. Toxicol. 15 doi:http://dx.doi.org/10.1021/tx015574b.
Daujat, M., Peryt, B., Lesca, P., Fourtanier, G., Domergue, J., Maurel, P., 1992. Omeprazole, an inducer of human CYP1A1 and 1A2, is not a ligand for the Ah receptor. Biochem. Biophys. Res. Commun. 188, 820–825. doi:http://dx.doi.org/10.1016/0006-291X(92)91130-I.
de Montellano, P.R.O., 2018. 1-Aminobenzotriazole: a mechanism-based cytochrome p450 inhibitor and probe of cytochrome p450 biology. Med. Chem. (Los Angeles) 8, 38–65. doi:http://dx.doi.org/10.4172/2161-0444.1000495.
Denisov, I.G., Frank, D.J., Sligar, S.G., 2009. Cooperative properties of cytochromes P450. Pharmacol. Ther. 124, 151–167. doi:http://dx.doi.org/10.1016/j.pharmthera.2009.05.011.
Easterbrook, J., Lu, C., Sakai, Y., Li, A.P., 2001. Effects of organic solvents on the activities of cytochrome p450 isoforms, UDP-dependent glucuronyl transferase, and phenol sulfotransferase in human hepatocytes. Drug Metab. Dispos. 29, 141–144.
FDA Adverse Event Reporting System (FAERS) Public Dashboard [WWW Document], 2020. U.S. Food and Drug Administration. . https://www.fda.gov/drugs/questions-and-answers-fdas-adverse-event-reporting-system-faers/fda-adverse-event-reporting-system-faers-public-dashboard.
Gabriel, S.E., Crowson, C.S., Campion, M.E., O'Fallon, W.M., 1996. Indirect and nonmedical costs among people with rheumatoid arthritis and osteoarthritis compared with nonarthritic controls. J. Rheumatol. 24, 43–48.
Gschwend, M.H., Erenmemisoglu, A., Martin, W., Tamur, U., Kanzik, I., Hincal, A.A., 2007. Pharmacokinetic and bioequivalence study of meloxicam tablets in helathy male subjects. Arzneimittelforschung 57, 264–268.
Hartman, J.H., Knott, K., Miller, G.P., 2014. CYP2E1 hydroxylation of aniline involves negative cooperativity. Biochem. Pharmacol. Biochem. Pharmacol. 87, 523–533.
Horn, J.R., Hansten, P.D., 2011a. Get to know an enzyme: CYP1A2 [WWW document]. Pharmacy Times, . https://www.pharmacytimes.com/publications/issue/2007/2007-11/2007-11-8279.
Horn, J.R., Hansten, P.D., 2011b. Get to know an enzyme: CYP2C9 [WWW document]. Pharmacy Times, . https://www.pharmacytimes.com/publications/issue/2008/2008-03/2008-03-8462.
Jean, D.J.S., Fotsch, C., 2012. Mitigating heterocycle metabolism in drug discovery. J. Med. Chem. 55, 6002–6020. doi:http://dx.doi.org/10.1021/jm300343m.
Kawakami, H., Ohtsuki, S., Kamiie, J., Suzuki, T., Abe, T., Terasaki, T., 2011. Simultaneous absolute quantification of 11 cytochrome P450 isoforms in human liver microsomes by liquid chromatography tandem mass spectrometry with in silico target peptide selection. J. Pharm. Sci. 100, 341–352. doi:http://dx.doi.org/10.1002/jps.22255.
Kedderis, G.L., n.d. The role of the mixed-function oxidase system in the toxication and detoxication of chemicals: Relationship in chemical interactions, Toxic Interactions. Academic Press, San Diego, 52–54.
Khojasteh, S.C., Prabhu, S., Kenny, J.R., Halladay, J.S., Lu, A.Y.H., 2011. Chemical inhibitors of cytochrome P450 isoforms in human liver microsomes: a re-evaluation of P450 isoform selectivity. Eur. J. Drug Metab. Pharmacokinet. 36, 1–16. doi:http://dx.doi.org/10.1007/s13318-011-0024-2.
Koonrungsesomboon, N., Khatsri, R., Wongchompoo, P., Teekachunhatean, S., 2017. The impact of genetic polymorphisms on CYP1A2 activity in humans : a systematic review and meta-analysis. Pharmacogenomics J. doi:http://dx.doi.org/10.1038/s41397-017-0011-3.
Krusekopf, S., Roots, I., Hildebrandt, A.G., Kleeberg, U., 2003. Time-dependent transcriptional induction of CYP1A1, CYP1A2 and CYP1B1 mRNAs by H+/K+-ATPase inhibitors and other xenobiotics. Xenobiotica 33, 107–118. doi:http://dx.doi.org/10.1080/0049850210000239 78.
Kumar, S., Patil, M.T., Kataria, R., Salnuke, D.B., 2016. Thiazole: a privileged scaffold in drug discovery. Chemical Drug Design, .
Linder, C.D., Renaud, N.A., Hutzler, J.M., 2009. Is 1-aminobenzotriazole an appropriate in vitro tool as a nonspecific cytochrome P450 inactivator. Drug Metab. Dispos. 37, 10–13. doi:http://dx.doi.org/10.1124/dmd.108.024075.
LiverTox [WWW Document], 2018. U.S. National Library of Medicine. National Institutes of Health. https://livertox.nih.gov/.
Mizutani, T., Yoshida, K., Kawazoe, S., 1992. Possible role of thioformamide as a proximate toxicant in the nephrotoxicity of thiabendazole and related thiazoles in glutathione-depleted mice: structure-toxicity and metabolic studies. Chem. Res. Toxicol. 6, 174–179. doi:http://dx.doi.org/10.1021/tx00032a006.
Mizutani, T., Yoshida, K., Kawazoe, S., 1994. Formation of toxic metabolites from thiabendazole and other thiazoles in mice: identification of thioamides as ring cleavage products. Drug Metab. Dispos. 22, 750–755.
Mobic [label], 2000.
Neal, R.A., Halpert, J., 1982. Toxicology of thiono-sulfur compounds. Annu. Rev. Pharmacol. Toxicol. 22, 321–330.
Nirogi, R., Palacharla, R.C., Uthukam, V., Manoharan, A., Srikakolapu, S.R., Kalaikadhiban, R.K., Boggavarapu, R.K., Ajjala, D.R., Bhyrapuneni, G., 2015. Chemical inhibitors of CYP450 enzymes in liver microsomes: combining selectivity and unbound fractions to guide selection of appropriate concentration in phenotyping assays. Xenobiotica 45, 95–106. doi:http://dx.doi.org/10.3109/00498254.2014.945196.
Obach, R.S., Kalgutkar, A.S., Ryder, T.F., Walker, G.S., 2008. In vitro metabolism and covalent binding of enol-carboxamide derivatives and anti-inflammatory agents sudoxicam and meloxicam : insights into the hepatotoxicity of Sudoxicam. Chem. Res. Toxicol. 1890–1899.
Rostom, A., Goldkind, L., Laine, L., 2005. Nonsteroidal anti-inflammatory drugs and hepatic toxicity: a systematic review of randomized controlled trials in arthritis patients. Clin. Gastroenterol. Hepatol. 3, 489–498.
Roth, S.H., 2001. Arthritis therapy: a better time, a better day. Rheumatology 40, 603–606.
Shirasaka, Y., Sager, J.E., Lutz, J.D., Davis, C., Isoherranen, N., 2013. Inhibition of CYP2C19 and CYP3A4 by omeprazole metabolites and their contribution to drug-drug interactions. Drug Metab. Dispos. 41, 1414–1424.
Spaggiari, D., Geiser, L., Daali, Y., Rudaz, S., 2014. Phenotyping of CYP450 in human liver microsomes using the cocktail approach. Anal. Bioanal. Chem. 406, 4875–4887. doi:http://dx.doi.org/10.1007/s00216-014-7915-4.
Staerkel, P., Horsmans, Y., 1999. Meloxicam-induced liver toxicity. Acta Gastroenterol. Belg. 62, 255–256.
Tornio, A., Neuvonen, P.J., Backman, J.T., 2006. The CYP2C8 inhibitor gemfibrozil does not increase the plasma concentrations of zopiclone. Eur. J. Clin. Pharmacol. 62, 645–651. doi:http://dx.doi.org/10.1007/s00228-006-0155-6.
Wiseman, E.H., Chiaini, J., 1972. Anti-inflammatory and pharmacokinetic properties of sudoxicam N-(2-thiazolyl)-4-hydroxy-2-methyl-2H-1,2-benzothiazine-3-carboxamide 1,1-dioxide. Biochem. Pharmacol. 21, 2323–2334. doi:http://dx.doi.org/10.1016/0006-2952(72)90383-8.
Woods, C.M., Fernandez, C., Kunze, K.L., Atkins, W.M., 2011. Allosteric activation of cytochrome P450 3A4 by α-Naphthoflavone: branch point regulation revealed by isotope dilution analysis. Biochemistry 50, 10041–10051. doi:http://dx.doi.org/10.1021/bi2013454.
Xu, J., Morisseau, C., Hammock, B.D., 2014. Expression and characterization of an epoxide hydrolase from Anopheles gambiae with high activity on epoxy fatty

acids. Insect Biochem. Mol. Biol. 54, 42–52. doi:http://dx.doi.org/10.1016/j.ibmb.2014.08.004.
Yocum, D., Fleischmann, R., Dalgin, P., Caldwell, J., Hall, D., Roszko, P., 2000. Safety and efficacy of meloxicam in the treatment of osteoarthritis: a 12-week, double-blind, multiple-dose, placebo-controlled trial. Arch. Intern. Med. 160, 2947–2954. doi:http://dx.doi.org/10.1001/archinte.160.19.2947.
Yu, A., Haining, R.L., 2001. Comparative contribution to dextromethorphan metabolism by cytochrome P450 isoforms in vitro: can dextromethorphan be used as a dual probe for both CYP2D6 and CYP3A activities? Drug Metab. Dispos. 29, 1514–1520.
Zhang, Z.-Y., 2014. Sudoxicam. Handbook of Metabolic Pathways of Xenobiotics, .